Technical Report

TR-13-25

Influences of load variations on the plastic deformation in friction stir welds and contour slits in copper shells

Lai-Zhe Jin, Rolf Sandström

Materials Science and Engineering, KTH

December 2013

Svensk Kärnbränslehantering AB
Swedish Nuclear Fuel
and Waste Management Co

Box 250, SE-101 24 Stockholm
Phone +46 8 459 84 00

ISSN 1404-0344
SKB TR-13-25

ID 1413602

Updated 2017-08

Influences of load variations on the plastic deformation in friction stir welds and contour slits in copper shells

Lai-Zhe Jin, Rolf Sandström

Materials Science and Engineering, KTH

December 2013

Keywords: Elasto-plastic analysis, Copper, Canister, Slit, Stress concentration, Pressure gradient.

This report concerns a study which was conducted for SKB. The conclusions and viewpoints presented in the report are those of the authors. SKB may draw modified conclusions, based on additional literature sources and/or expert opinions.

A pdf version of this document can be downloaded from www.skb.se.

Update notice

The original report, dated December 2013, was found to contain factual errors which have been corrected in this updated version. The corrected factual errors are presented below.

Updated 2017-08

Location	Original text	Corrected text
Page 9, last paragraph	*New text inserted*	The flow curves presented in Figure 2-1 with reference to Sandström et al. 2013b (SKB R-13-33), were taken from a preliminary version of that report. In the finally printed, revised, R-13-33, Figure 6-6 illustrates such curves, but built on slightly other parameter values. There is thus no reference to the precise material properties used in the calculations in the report TR-13-25, but they are deemed reasonable by the authors of R-13-33.

Abstract

With constitutive equations developed from slow strain rate tensile testing data on weld zones, elasto-plasticity analyses with contact modelling of friction stir welded canister copper shell under even and uneven load cases have been performed at a temperature of 75°C. In contrast to the even load case where a uniform pressure of 15 MPa acts on the copper shell surface, the uneven load cases assume that canisters are exposed to isostatic pressure of 7.4 MPa on the lid and 19 MPa on the base but with two different distributions of normal and shear stresses. The loading is applied gradually to simulate the expected behaviour in the repository. Since the difference in mechanical properties between the weld zones and the parent metal is small and the von Mises stress does not exceed 100 MPa, no creep damage will initiate in the weld zones.

The roots of the contour slits are the most heavily stressed parts of the canister copper shell, particularly the lower roots of contour slits for unevenly loaded canisters. The maximum von Mises stress is 216 to 238 MPa. This gives rise to significant local deformation but since the stresses perpendicular to the slits in these regions are compressive, no creep damage will appear.

Contents

1 Introduction 7

2 Model formulation 9
2.1 Elasto-plasticity analysis 9
2.2 Material modelling 9
2.3 Geometry modelling 10
2.4 Load cases 11
2.5 Contact modelling 12
2.6 Model definition and computation 13

3 Deformation in copper shells 15
3.1 Lid and base 16
3.2 Copper cylinder 17
3.3 Weldments 19
3.4 Slits 21

4 Discussion 29

5 Conclusions 31

Acknowledgements 33

References 35

1 Introduction

In Sweden spent nuclear fuel is planned to be deposited in granitic rock according to the KBS-3 concept (Raiko et al. 2010). The repository will provide a multi-barrier protection consisting of a waste package, a low permeability bentonite buffer, and the rock mass against the spreading of radioactive nuclides in the environment. The waste package for encapsulating the spent nuclear fuel is composed of two parts: a load carrying cast iron insert with channels for storing the spent fuel and a corrosion-resistant copper shell to prevent the waste package from chemical damage. The copper shell is a friction stir welded structure with a hot extruded or pierce-and-drawn tube, a forged lid and base. They are made of 30–100 ppm phosphorus alloyed oxygen free copper (Cu-OFP). A longitudinal section drawing of the waste package is illustrated in Figure 1-1. It should be noticed that the waste package will most likely be placed vertically in reality. At the connections between the lid/base and the tube, there exist slits of about 75 mm in length and 0.16–0.3 mm in width, which are marked with circles in Figure 1-1 and drawn in Figure 1-2 in detail. In addition, there are 2 +1.1/–0.3 mm axial gap between steel and copper lids and 1.5 +0.25/–0.5 mm radial gaps between the copper shell and the insert owing to the manufacturing tolerances. In the computation the gaps have been assumed to be 2 and 1.5 mm, respectively.

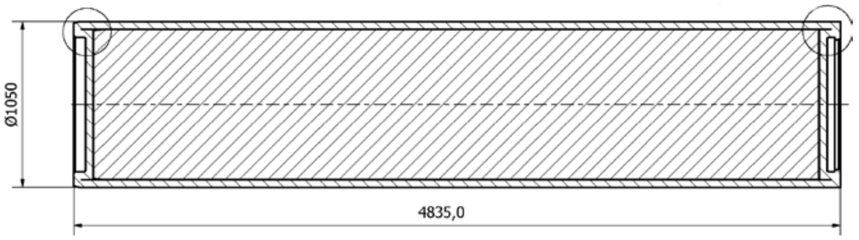

Figure 1-1. *Longitudinal section drawing of the waste package, dimensions in mm. The backslash represents the friction stir welded copper shell and the forward slash the cast iron insert.*

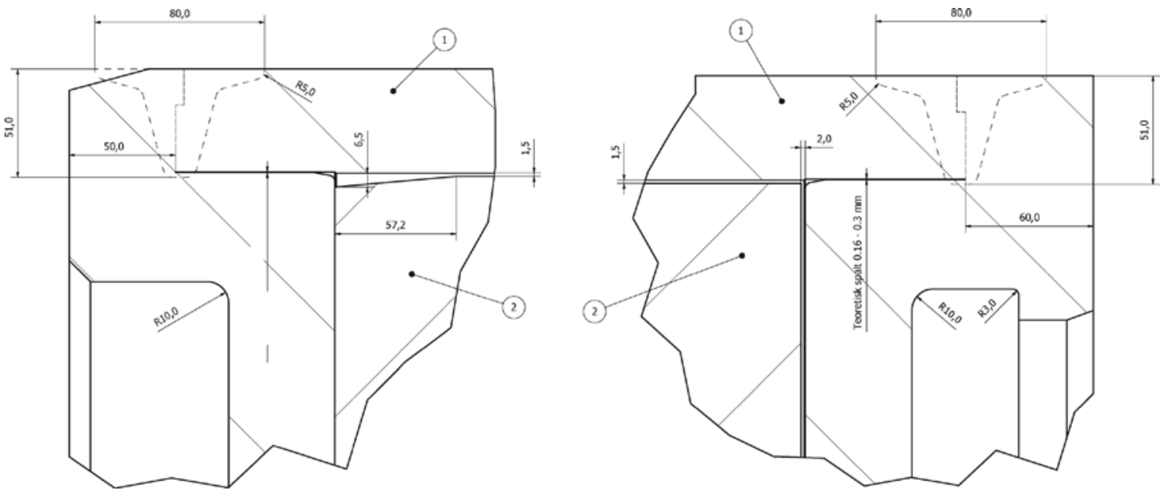

Figure 1-2. *Details of lower (left) and upper (right) section drawings of waste package in mm. Marks 1 and 2 refer to copper shell and insert respectively. The slits are horizontal and in the centre of the drawings. The positions of the welds are illustrated with dashed lines.*

After the spent nuclear fuel is placed into the channel tubes of the cast iron insert, the copper shell will be sealed by friction stir welding and then permanently deposited into a granitic rock repository at a depth of about 500 m. Sodium bentonite MX-80 of low permeability or a bentonite with similar properties will fill the space between the waste package and the rock mass (Raiko et al. 2010). During the storage, water will reach the repository from the underground layer of the water-bearing permeable rock due to the hydraulic gradient induced by the difference in elevation. The water flow in turn wets the bentonite buffer and develops a swelling pressure inside the buffer. As an object submerged in the bentonite buffer, the canister is thus mechanically loaded and supported by the bentonite buffer. The postulated load acting on the canister surface consists of a hydraulic pressure of about 4 MPa in combination with a swelling pressure of 11 MPa (Raiko et al. 2010). The latter corresponds to a nominal density of 2,050 kg/m^3 at temperatures of 10–70°C. Under such an external pressure, plastic deformation will take place in the copper shell. The lid, the base, and the cylinder wall will be pressed against the iron insert (Jin and Sandström 2009). Two important aspects about the deformation of the copper shell have not been studied in detail before: Firstly, the creep properties of the welds are different from those of the parent metal (Sandström et al. 2013a, b). Secondly, the slit contours will be distorted and local stress concentrations will develop. Such plastic deformation in friction stir welds and contour slits for copper shells will be analysed.

An approximately evenly distributed load on the copper shell will be the normal situation. However, the load acting on the copper shell surface may be unevenly distributed in some cases due to the unevenness in the rock contour and variation in geometry and density of the buffer blocks. Such an unevenly distributed swelling pressure may remain permanent on the copper shell surface due to the friction induced density differences and incomplete buffer homogenisation. An additional reason for the uneven swelling pressure is the conversion of sodium bentonite MX-80 to calcium bentonite MX-80Ca. This may occur in contact with calcium-rich groundwater where the sodium ions in the bentonite buffer are gradually exchanged by calcium ions. After the ion replacement, the maximum swelling pressure in the calcium bentonite buffer could approach a value as high as 15 MPa, which is 4 MPa higher than the maximum swelling pressure in the sodium bentonite buffer. Then the axial force equilibrium of the copper shell can only be taken up by the vertical bentonite contact surfaces to the bedrock and the copper shell inducing shear stresses (Raiko et al. 2010, Börgesson et al. 1995, 2010, SKBdoc 1206894). Under the stress gradients, it is expected that the deformation of the copper shell and particularly the slit contours will be somewhat different from the evenly distributed load case. Such an influence of swelling pressure gradient on the stress evolution in copper shell needs to be carefully analysed.

The purpose of the present report is to study influences of load variations on the stress and strain evolution in friction stir welds as well as in the contour slits and to identify the difference between load cases. Since the increase in hydraulic and swelling pressures in the bentonite buffer is expected to be gradual, the copper shell will be exposed to a slowly increasing load. Thus, the constitutive isotropic hardening equations deduced from the slow strain rate tensile testing data have been adopted in the material modelling in the finite element elasto-plasticity analyses. It has been shown that the constitutive equations are consistent with creep data and the primary creep curves have successfully been derived from the slow strain rate tensile testing data (Sandström and Hallgren 2012).

2 Model formulation

2.1 Elasto-plasticity analysis

A model on the basis of Navier's equations of elasticity in conjunction with the isotropic strain hardening is employed to simulate the finite strain elasto-plastic deformation in the copper shell.

By writing the elastic left Cauchy-Green tensor and the plastic right Cauchy-Green tensor as a function of deformation gradient tensor $\boldsymbol{F}$ (in its total F and plastic part F_p), and using the rule of multiplicative decomposition for elastic and plastic deformation, the plastic flow rule can be expressed as.

$$-\frac{1}{2}\left(\dot{F}_\mathrm{p}^{-1}F_\mathrm{p}^{-T}+F_\mathrm{p}^{-1}\dot{F}_\mathrm{p}^{-T}\right)=\lambda F_\mathrm{p}^{T}\frac{\partial Q_\mathrm{p}}{\partial\tau}FF_\mathrm{p}^{-1}F_\mathrm{p}^{-T} \tag{2-1}$$

where: λ is the plastic multiplier, $\boldsymbol{Q}_\mathrm{p}$ the plastic potential, and τ is the stress. λ and $\boldsymbol{Q}_\mathrm{p}$ should satisfy the Kuhn-Tucker conditions:

$$\lambda\geq 0 \qquad \boldsymbol{Q}_\mathrm{p}\leq 0 \qquad \lambda\boldsymbol{Q}_\mathrm{p}=0 \tag{2-2}$$

After integrating the flow rule in Equation (2-1), the plastic Green-Lagrange strain tensor $\varepsilon_\mathrm{p}=\frac{1}{2}\left(\boldsymbol{F}_\mathrm{p}^{T}\boldsymbol{F}_\mathrm{p}-\boldsymbol{I}\right)$ is derived from the plastic deformation gradient tensor, and the elastic Green-Lagrange strain tensor $\varepsilon_\mathrm{e}=\frac{1}{2}\left(\boldsymbol{F}_\mathrm{e}^{T}\boldsymbol{F}_\mathrm{e}-\boldsymbol{I}\right)$ is computed from the elastic deformation gradient tensor $\boldsymbol{F}_\mathrm{e}=\boldsymbol{F}\,\boldsymbol{F}_\mathrm{p}^{-1}$. The subscript p stands for the plastic component and e for elastic component.

2.2 Material modelling

By considering the contributions of work hardening, dynamic recovery, and static recovery to the change of the dislocation density and in turn to the material strength (Sandström and Hallgren 2012), an expression of true stress-strain curve, written as $\sigma=\sigma_0[1-\exp(-\omega\varepsilon/2)]$ with σ being the Cauchy stress, ε the true strain, and σ_0 and ω constants, was derived for Cu-OFP. By taking the temperature and strain rate dependence of the parameters of σ_0 into account in the appropriate way, it has been demonstrated that the equation can describe stress strain curves over a wide range of conditions for parent metals (Sandström and Hallgren 2012). More recently these results have been expanded to welds, and constitutive equations for the thermo-mechanically affected zone (TMAZ) and the heat affected zone (HAZ) have been set up (Sandström et al. 2013a, b). According to Sandström et al. (2013b), the yield strength for the parent metal were evaluated as 65.1 MPa and the flow curve parameters as $\sigma_0=153.8$ MPa, and $\omega=14.67$ respectively at a temperature of 75°C and a strain rate of 10^{-8} s^{-1}. The latter corresponds to a loading time of about 1 year. If a loading time of for example 100 years would have been used, this would have given marginally lower stresses and larger strains. In the computation, a gradual loading was applied to simulate the expected situation in the repository. The applied pressure has increased linearly with log time. The corresponding flow curve parameters for TMAZ and HAZ were identified as $\sigma_0=153.2$ MPa and $\omega=11.73$ in conjunction with yield strengths of 86.8 and 84.6 MPa, respectively. With these parameters, the flow curves of TMAZ, HAZ, and parent metal were generated. They are presented in Figure 2-1. An important feature of TMAZ and HAZ is that they are harder than parent Cu-OFP. The weld zones have higher yield strength than the parent metal. Although the weld zones initially have lower work hardening rates, their flow curves are above that of the parent metal for all strains. Both TMAZ and HAZ are assumed to have an elastic modulus of 109 GPa and a Poisson's ratio of 0.308 at 75°C, which are the same values as for parent Cu-OFP.

The flow curves presented in Figure 2-1 with reference to Sandström et al. 2013b (SKB R-13-33), were taken from a preliminary version of that report. In the finally printed, revised, R-13-33, Figure 6-6 illustrates such curves, but built on slightly other parameter values. There is thus no reference to the precise material properties used in the calculations in the report TR-13-25, but they are deemed reasonable by the authors of R-13-33.

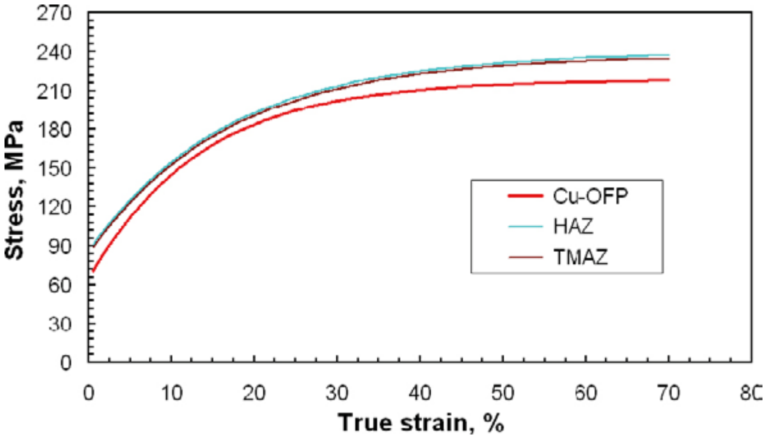

Figure 2-1. *Representation of true stress-strain hardening curves for parent metal and weld zones at 75°C and* $1 \cdot 10^{-8}$ s^{-1} *(Sandström et al. 2013b).*

2.3 Geometry modelling

Geometry modelling takes a diameter of 1,050 mm, a wall thickness of 50 mm, and a length of 4,835 mm as the dimensions of a friction stir welded copper shell. Due to the existence of symmetry with respect to the copper shell's vertical axis z in cylindrical coordinates (r, φ, z), the geometry is modelled with a half plane at angular $\varphi = 0$ and radial distance $r \geq 0$. The heat affected zone (HAZ) and thermo-mechanically affected zone (TMAZ), as illustrated in Figure 2-2, are modelled as a 50 to 100 mm thick parabola (Andersson et al. 2007). The 75 mm long slit with a latitudinal dimension of 0.16 mm is modelled so that its base is cut by the HAZ. The possible mesh singularity is avoided by filleting the sharp corners induced by the HAZ at the slit root, see Figure 2-4.

The length and the radius of the cast iron insert are modelled as 2 and 1.5 mm, respectively smaller than the axial and radial inner dimensions of the copper shell. The weight of the simulated copper shell, cast iron insert, and spent nuclear fuel are 7,500, 13,700, and 3,500 kg, respectively (SKB 2010). It is assumed that there is a neutral plane across the copper shell wall on which its normal component is equal to zero. The coordinate z for this plane is determined by multiple elastic computations with given geometry.

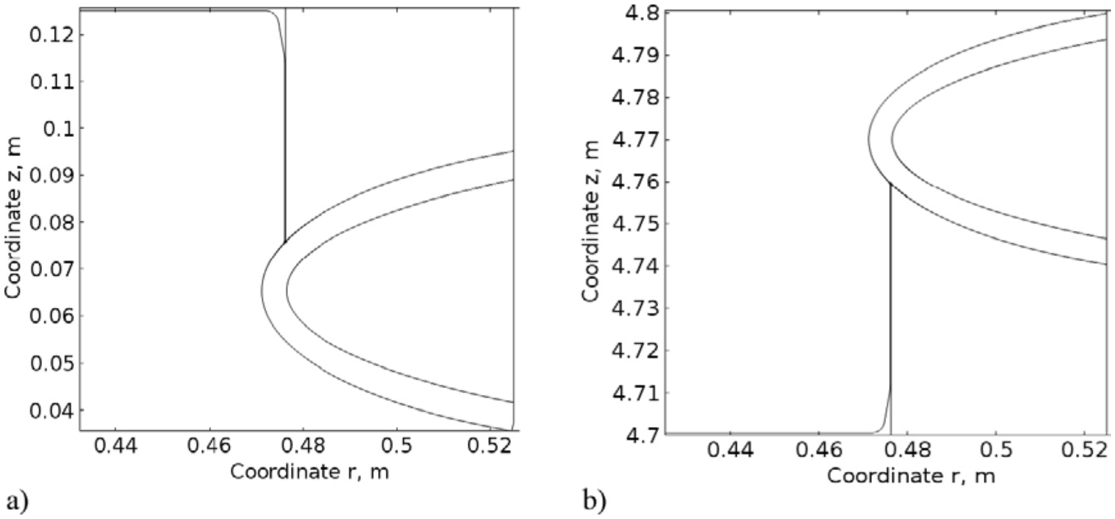

Figure 2-2. *Enlarged view of slit and weld trace in the copper shell; a) between the base (left) and the tube (right); b) between the lid (left) and the tube (right)*

2.4 Load cases

It may occur in the deposition hole that the density of the MX-80 bentonite buffer just above the canister is 1,950 kg/m^3 and the bentonite buffer just below the canister submerges in calcium-rich ground water (SKBdoc 1206894). The decrease of density in the upper half buffer is also considered possible if there is rock fall out in the upper parts and upward swelling of the buffer against a dry backfill, which will cause a decrease in buffer density in the upper parts. The corresponding maximum swelling pressures of 3.4 and 11 MPa respectively for the buffer density of 1,950 and 2,050 kg/m^3 can be calculated through the expression of swelling pressure (Börgesson et al. 2010)

$$\sigma = \sigma_0 \left(\frac{e}{e_0} \right)^{\frac{1}{\beta}} \tag{2-3}$$

where β is –0.19, e_0 the reference void ratio of 1.1, and σ_0 is the swelling pressure at e_0 in conjunction with the current void ratio

$$e = (\rho_s - \rho_m)/(\rho_m - \rho_w) \tag{2-4}$$

where ρ_m is the density at water saturation, ρ_s the density of solids (2,780 kg/m^3), and ρ_w is the density of water (1,000 kg/m^3). In contact with calcium-rich ground water the sodium ions in the lower half of the bentonite buffer MX-80 in the deposition hole may be exchanged and replaced by calcium ions, which could result in calcium converted MX-80 or MX-80Ca. The consequence of such an ion replacement will raise buffer density and in turn enhance the maximum swelling pressure from 11 MPa to 15 MPa (SKBdoc 1206894). Thus, swelling pressures of 3.4 and 15 MPa emerge on the copper shell lid and base, respectively. With a strong swelling pressure gradient along the vertical axis, the axial force equilibrium in the copper shell can only be achieved by the existence of axial shear stresses originating from the friction between the copper shell surface and the saturated bentonite. With an assumption of linear variation of swelling pressure along the vertical axis, the vertical shear stresses on the surface of copper shell wall are determined by the expression

$$\tau = \sigma \tan \varphi \tag{2-5}$$

where σ is the current swelling pressure and φ is the friction angle. The critical friction angle that limits the density gradient to a value without buffer homogenisation is $\varphi = 10°$ for MX-80 at high densities (Börgesson et al. 2010). Two critical load cases, both sustaining swelling pressures of 3.4 MPa on the lid and 15 MPa on the base and hydraulic pressure of 4 MPa but with different swelling pressure and shear stress distributions, are presented below.

Load case 1 that is presented in Figure 2-3a has been proposed in SKBdoc 1206894. In this load case, the axial force equilibrium to the copper shell is established by ensuring the sum of shear force acting on the copper shell wall according to Equation (2-5) being equal to the difference in normal force acting on the lid/base without the loss in shear stresses. For this reason, a friction angle $\varphi = 3.94°$ that is lower than the friction angle at failure has been chosen to satisfy the axial force equilibrium. The combined pressures $\sigma_1 = 19$ MPa and $\sigma_2 = 7.4$ MPa, and shear stresses $\tau_1 = 1.031$ MPa and $\tau_2 = 0.232$ MPa with an assumption of linear variation of swelling pressure along the vertical axis are illustrated in Figure 2-3a.

In load case 2, which has also been proposed in SKBdoc 1206894, a critical friction angle $\varphi = 10°$ is employed as mentioned before. The difference in comparison to the load case 1 is that the axial length along which the loss in shear stress is determined by the force equilibrium. Shear stresses from $\tau_1 = 2.5$ MPa to $\tau_2 = 0.573$ MPa and an axial length of 1.96 m from the base are required to achieve the axial force equilibrium. The maximum and minimum shear stresses are taken from Equation (2-5). With combined pressure $\sigma_1 = 19$ MPa acting on the copper shell base and $\sigma_2 = 7.4$ MPa acting on the top, as shown in Figure 2-3b, the load case 2 represents a more severe load situation than load case 1, because the stress gradient at the base is 5.92 MPa/m, which should be compared to 2.39 MPa/m for load case 1.

As mentioned before, the deposition of waste package in granitic rock will generate a hydraulic pressure of 4 MPa from the groundwater and an evenly distributed swelling pressure of 11 MPa from completely water saturated and consolidated bentonite on the copper shell surface. Sustaining such a combined load of 15 MPa was adopted as a design criterion for the copper shell (Raiko et al. 2010). In this study, it is referred to as load case 0.

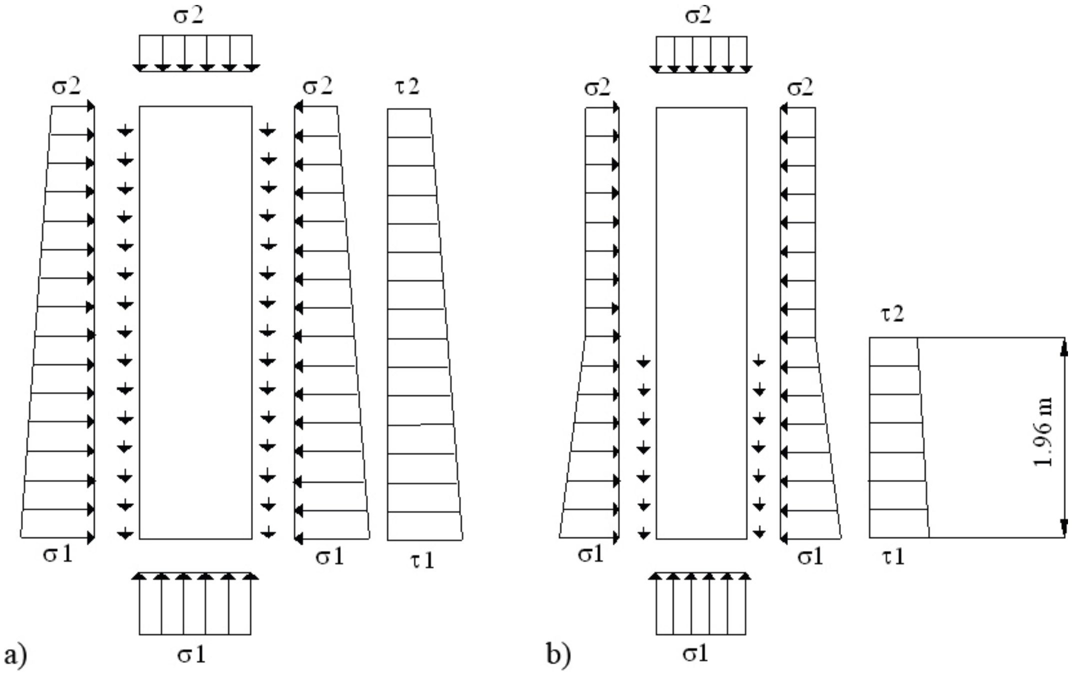

Figure 2-3. Distribution of normal and shear stresses on the interface between the copper shell and the buffer; a) load case 1; b) load case 2.

2.5 Contact modelling

With a sufficient pressure imposed on the outer surface of the copper shell, the lid/base and the cylindrical wall will deflect inward as the dimensions of the cast iron insert are smaller than that of the copper shell. The allowable inward deflection according to the manufacturing tolerance in the computations are taken as 2 mm in the axial direction and 1.5 mm in the radial direction, which will cause contact and contour distortion particularly in slits. From a computational point of view, it is necessary to prevent the contact surfaces to penetrate each other. With the assumption that the cast iron insert is rigid, the penalty-barrier method has been applied to the FEM-model as was done in Jin and Sandström (2008, 2009). The contact pressure P_n on the boundary can be expressed as

$$p_n = \begin{matrix} \kappa_n - e_n \cdot g & g < 0 \\ \kappa_n \cdot \exp\left(-g \cdot e_n / \kappa_n\right) & g \geq 0 \end{matrix} \qquad (2\text{-}6)$$

where κ_n is the input estimation of normal stress, e_n the penalty stiffness, and g is the width of the gap. In the method, additional stiffness acting as a nonlinear spring connects the surface to be contacted. During periods of non-contact it has low stiffness and hence has negligible effect on the deformation. As the gap between contact pair is reduced and approaches a predefined distance, the spring is activated and resists further closure. The force balance in a static state determines the possible gaps between the lid/base and the iron insert under the external pressure and the internal weight. The contact parameters in Equation (2-6) are obtained by iteration in an optimisation procedure where as hard springs as possible are looked for without jeopardising the convergence of the FEM computation. The resulting applied normal stresses and penalty stiffness as well as predefined gaps are listed in Table 2-1.

Table 2-1. Contact parameters for lid/base

Load case	Boundary	Inner lid	Inner base	Inner wall
For all cases	Penalty stiffness e_n, GPa m^{-1}	8,000	8,000	8,000
	Gap g, mm	1.00	1.00	1.50
Load case 0	Normal stress k_n, MPa	20.0	15.0	6.20
Load case 1	Normal stress κ_n, MPa	14.7	25.0	6.45, 6.4, 0.62
Load case 2	Normal stress κ_n, MPa	6	15.2	6.3, 6.25, 0.82

Due to linear variation of the swelling pressure along the vertical axis in load case 1 and 2, two linear equations thus three values are employed to describe the variation of gaps along the inner wall. The contact modelling in slits uses the software's built-in function with its given parameters. It is based on the same principles as described above, but the constants are found automatically.

2.6 Model definition and computation

The current elasto-plastic model is formulated and solved by the commercial software COMSOL Multiphysics version 4.3. Due to possible involvement of large plastic strains in the deformation of copper shells, the model is established by the Navier's equations in conjunction with an associated plastic flow rule written by the elastic left Cauchy-Green deformation tensor with multiplicative decomposition of deformation. A stationary solver with pseudo-time t as parameter is applied to solve the path dependent model by grouping elasto-plasticity and contact problems into different sub steps. A parallel sparse linear solver firstly computes the solution for the displacement variables while keeping the contact variables fixed. Then an augmented Lagrangian solver computes the contact variables while keeping the displacement field fixed. The solving procedure is repeated until a convergence criterion is met.

The isostatic pressures and shear stresses are incrementally imposed on the outer surface of the copper shell over a pseudo-time interval of 0.1 s, and the contact pressures of Equation (2-6) are also incrementally applied on the inner surfaces of the lid/base and the copper cylinder. Lagrange quadratic finite elements are employed in the current model. The mesh size differs in different positions. A fine mesh is assigned to the domains that cover the slit roots, weld lines, and contact boundaries. Relatively coarse meshes are used in other parts. The maximum and the minimum allowable triangular element size are 0.32 and $3.9 \cdot 10^{-6}$ m respectively for the geometry domain. Subsequently, the sub domains are partitioned by 104,244 triangular elements, 3,886 edge elements, and 66 vertex elements. Enlarged views of the triangular mesh idealisation around slit roots are presented in Figure 2-4.

In addition, a boundary layer mesh which is a mesh with dense element distribution in the normal direction is specified at slit boundaries albeit it is not shown in Figure 2-4. A value in the order of $1 \cdot 10^{-6}$ is specified for the relative tolerance of the estimated error in the solution. A total of 3,011,676 degrees of freedom are solved for in the model.

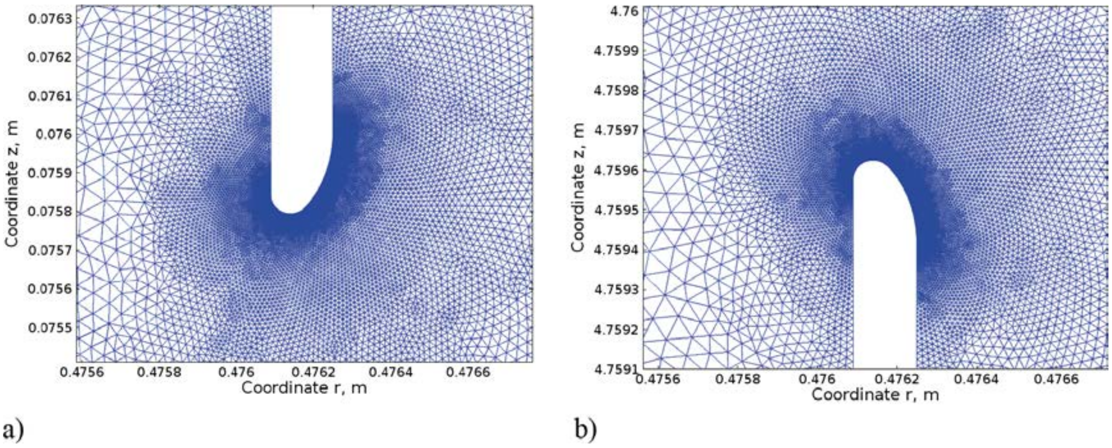

a) b)

Figure 2-4. *Triangular mesh idealisation around slit roots. Slit width 0.16 mm; a) lower slit; b) upper slit.*

3 Deformation in copper shells

Displacement and von Mises stress distributions for fully loaded copper shell are illustrated in Figures 3-1 and 3-2. Figure 3-1 shows that the inward displacement of copper cylinder differs between the load cases. The legend values in Figure 3-1a (case 0) show that the inward displacements in the copper cylinder wall are larger than in the lid/base. It means that the deformed cylindrical copper shell takes an hourglass shape with lid/base behaving as inward clamped disks and the cylindrical part being homogeneously deformed inward. In load case 1, the copper cylinder near the base touches the cast iron insert first, where the inward displacement is the largest. With load increment, the displacement gradually spreads upward while keeping tight contact with the insert. In load case 2, the inward displacement lies mainly at the lower part of the cylinder and no contact occurs in the upper part. Figure 3-2 indicates that von Mises stress in the major part of deformed copper cylinder is about 65 MPa or below. The illustrated von Mises stress distributions in the three load cases are not very different. Inspection of deformed canister in section 3.4 shows that similarly to the evenly loaded copper shell the maximum von Mises stress lies in the slit roots.

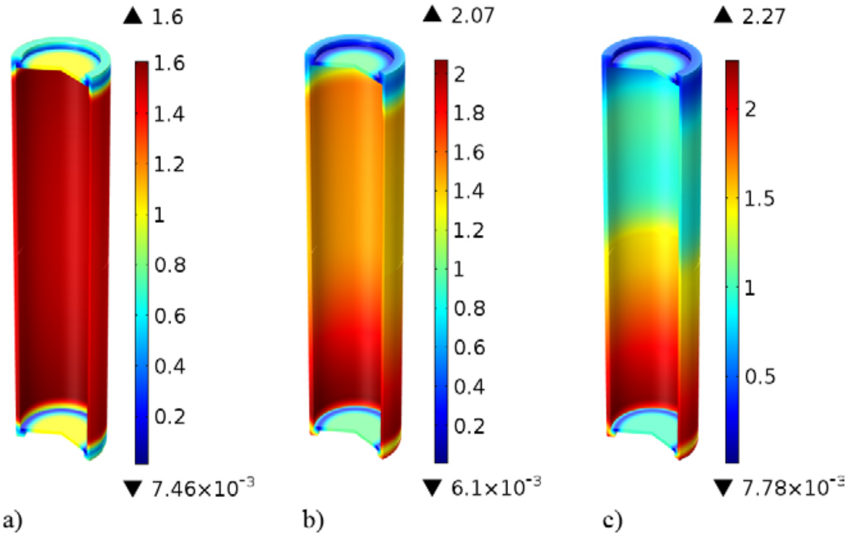

Figure 3-1. *Displacement distribution in copper shell, mm; a) load case 0; b) load case 1; c) load case 2.*

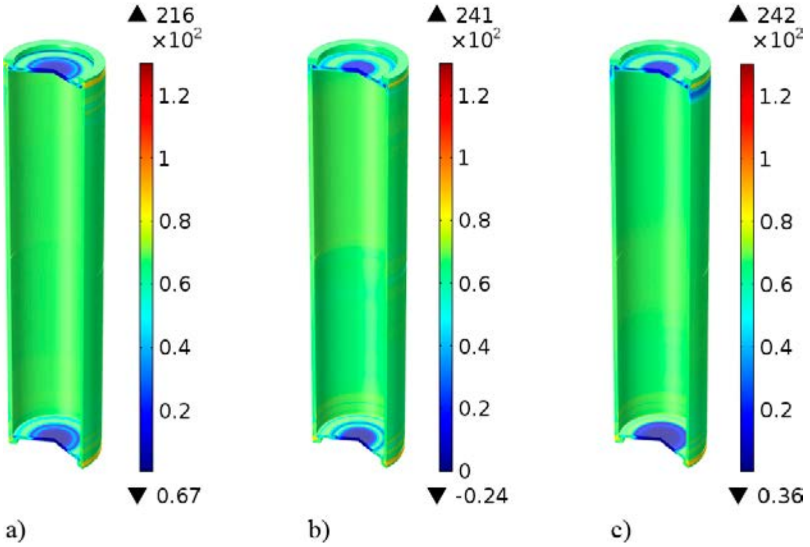

Figure 3-2. *von Mises stress distribution in copper shell, MPa; a) load case 0; b) load case 1; c) load case 2.*

3.1 Lid and base

Figure 3-3 illustrates the displacements of the lid/base under fully imposed loads for the three load cases as well as under a load of 1.5 MPa for load case 0. The computation indicates that the inner surface of the lid/base begins to touch the cast iron insert at the axial symmetry axis under a pressure of about 1.2 MPa. The contact length of the inner surface gradually extends over the copper shell radius with incremental loading. The figure shows that under fully imposed loads, all cases reach the allowable deflection of 1 mm; while the contact length of the inner surface gradually extends over the copper shell radius and finally approaches 0.31 m with the pressure rising from 1.5 to 19 MPa. This behaviour is in agreement with previous creep calculations although the total contact length was only 0.2 m then (Jin and Sandström 2009).

Such an inward deflection will inevitably attain a state of plastic deformation. Computation results indicate that pressures of 3.4 MPa and 3.8 MPa are required to initiate plastic yielding in the lid and base, respectively. The deflection induced plastic strains are shown in Figure 3-4. The maximum plastic strains of 0.82% appear in the base at about 0.465 m from the axial symmetry axis for load case 1 and 2. For the evenly loaded case, they take values of 0.54 and 0.39% in the lid and base, respectively. The second strain peaks of 0.17, 0.36, and 0.49% from load case 0 to 2 respectively emerge in the bases at positions where the curvature becomes significant. The corresponding plastic strains are only about 0.13% in the lid for load case 1 and 2 due to relatively small bending curvatures caused by a pressure of 7.4 MPa.

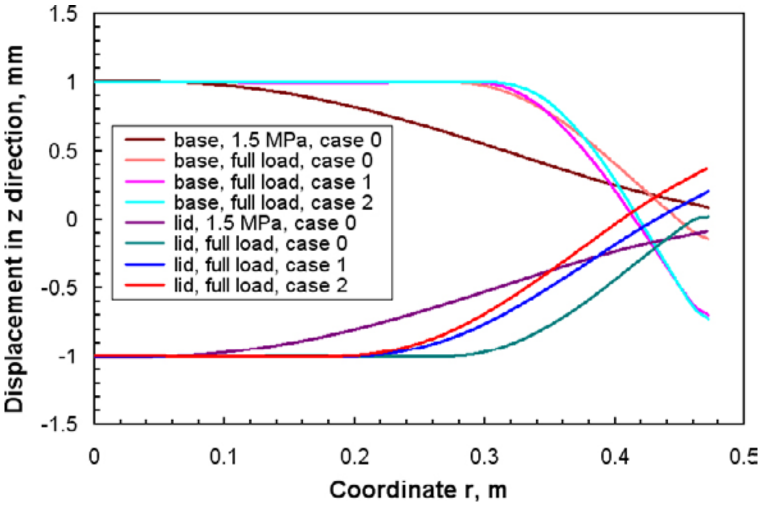

Figure 3-3. *Displacements of inner lid/base in direction of vertical axis of copper shell under fully imposed pressures as well as under 10% load for the even load case (case 0).*

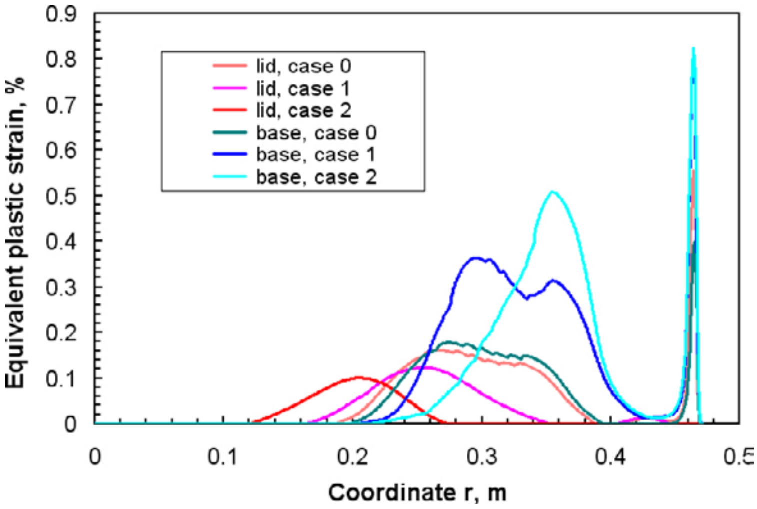

Figure 3-4. *Plastic strain distributions of inner lid/base along radial axis r under fully imposed pressures.*

3.2 Copper cylinder

Figures 3-5 to 3-7 show the deformation of the copper cylinder for the three load cases. Obviously, the deflection paths of unevenly loaded cases differ from the evenly loaded copper shell (Jin and Sandström 2009) albeit the maximum inward displacements of 1.5 mm are the same. With an even load acting on the outer surface, the copper cylinder uniformly deflects inward. The contact between the inner side of the copper cylinder and the cast iron insert occurs only when the pressure exceeds 7.5 MPa. This can be seen in Figure 3-5 where the radial displacements of the shell wall under incremental loading are illustrated. At the pressure of 8.4 MPa, the inner side of the copper cylinder has already fully touched the cast iron insert. Further load increment only increases the contact length between the copper shell wall and the cast iron insert. These findings are also in agreement with previous creep calculations (Jin and Sandström 2008). However in Jin and Sandström (2008), the contact with the insert only took place after long time. This was due to the use of an empirical model for primary creep that significantly underestimated the strain rate during this creep stage (Sandström and Andersson 2008).

In contrast to evenly loaded copper shell, inward deflection of the copper cylinder becomes uneven for load case 1 and 2, see Figures 3-6 and 3-7. The copper cylinder near the base deflects first and the deflection gradually spreads toward the upper sections. The figures show that contacts first appear at the *z*-coordinate 0.63 and 0.47 m and under about 46 and 50% of the fully imposed loads for case 1 and 2, respectively. It means that a pressure of 7.8 MPa for load case 1 and 8.1 MPa for load case 2 are required to get contact with the cast iron insert. These values are quite close to the critical pressure mentioned above for the evenly loaded copper shell. It well explains the observation in load case 2 that contact only occurs in the copper shell wall below 1.96 m and a full contact between the copper shell wall and the insert never appears. This is because the external pressure of 7.4 MPa for the z-coordinate 1.96 m and above is below the critical value of 8.1 MPa.

Although the deflection paths differ between the load cases, the computation results indicate that a minimum pressure of 6.7 MPa is required for both the even or uneven load cases to initiate plastic yielding in the copper cylinder. Plastic strain distributions along the inner wall of the copper tube for the three load cases are shown in Figure 3-8. Under fully imposed loads, plastic strains of 0.30, 0.51, and 0.55% appear at positions near the base respectively for the load case 0 to 2, respectively. However, for the rest of the contact region, the plastic strains are only about 0.27%. For load case 2, the plastic strains gradually decrease to zero above the z-coordinate of 1.8 m.

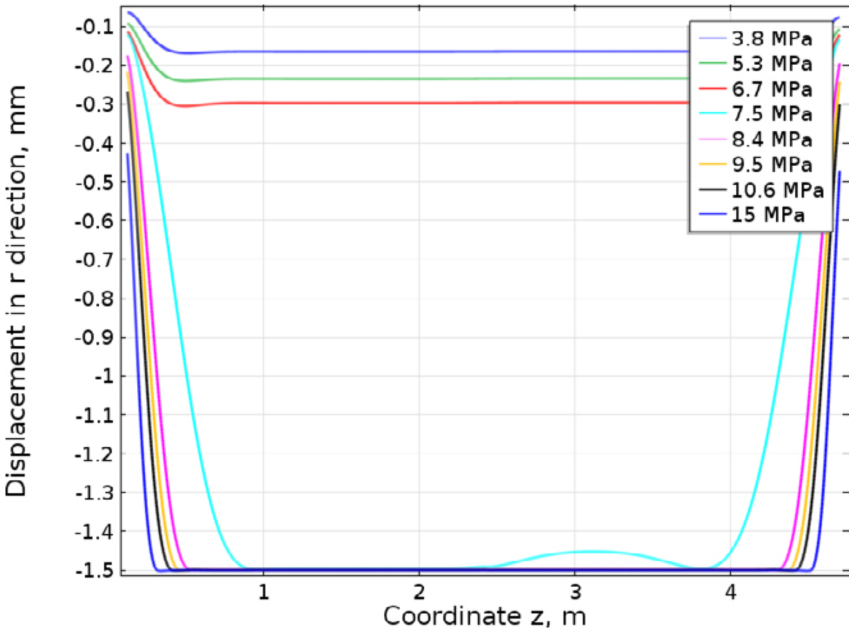

Figure 3-5. *Radial displacements of inner cylinder wall along vertical axis z with increment pressure for load case 0.*

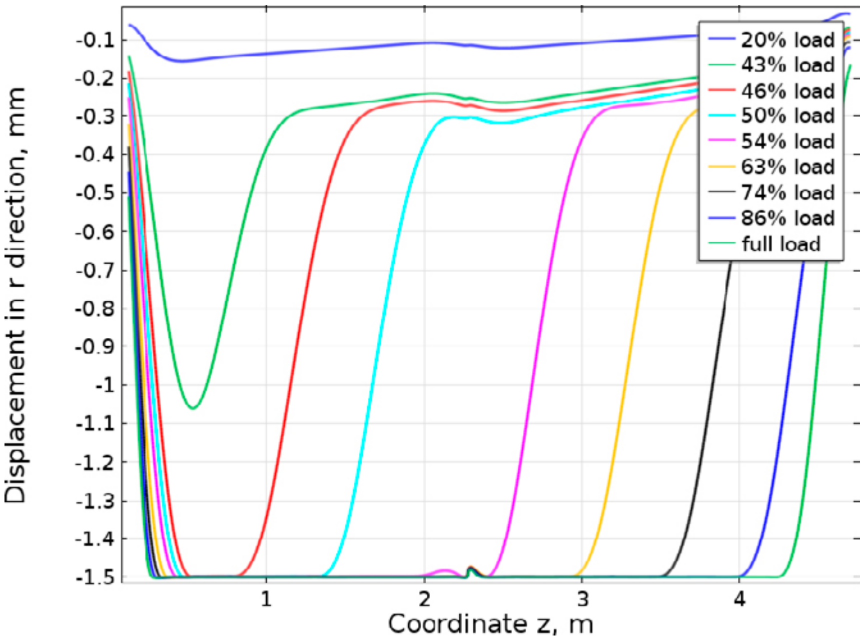

Figure 3-6. *Radial displacements of inner cylinder wall along vertical axis z with increment pressure for load case 1.*

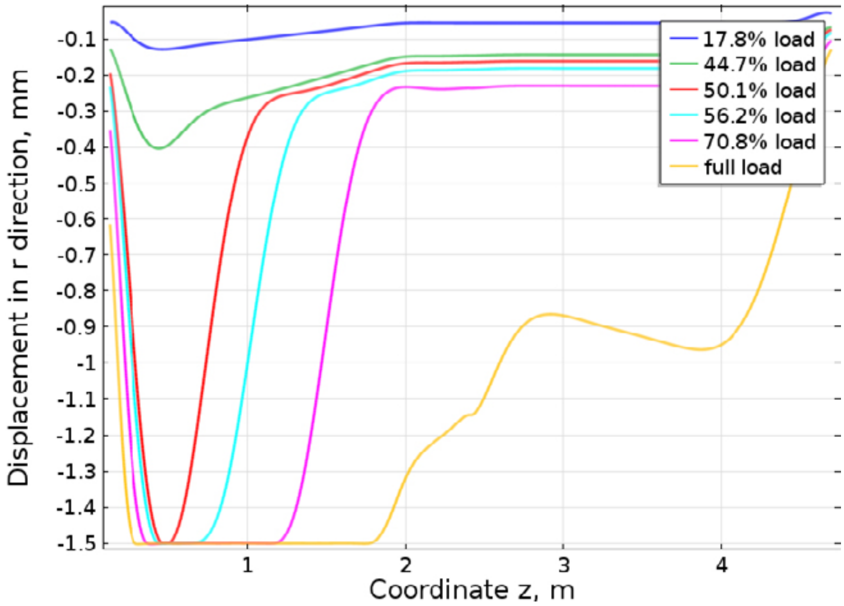

Figure 3-7. *Radial displacements of inner cylinder wall along vertical axis z with increment pressure for load case 2.*

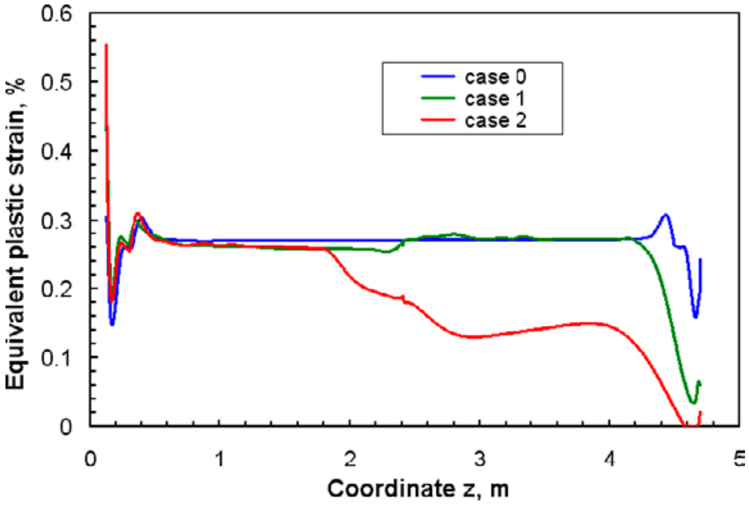

***Figure 3-8.** Plastic strain distribution of the inner wall of the copper tube along vertical axis z under fully imposed pressure.*

3.3 Weldments

Figures 3-9 to 3-11 illustrate the von Mises stress distributions in the weld zone from load case 0 to 2, respectively. The von Mises stresses in the heat affected zone (HAZ) are fairly constant and take values of about 90 MPa in the lower welds in all cases and in the upper welds in the even load case (case 0). This would give a creep rate that is negligibly small (Andersson et al. 2007). Outside the HAZ the stress is also fairly constant, taking values of about 65 MPa. The exception is at the slit root, which is discussed in the next section. In the thermomechanically affected zone (TMAZ) inside the parabolas, the von Mises stress is fairly homogeneous having values of 85 MPa or below, except for some areas with a stress of about 40 MPa. The stresses in the weld zones are thus slightly higher than in the surrounding copper shell. For the upper welds in the uneven load cases, most of the HAZ and TMAZ are covered by a von Mises stress of 50 MPa or below, except for small areas near the slit roots where stresses as high as 90 MPa can be observed. Outside the HAZ, the stresses are also rather constant having values of about 65 MPa or below.

The computed plastic strains in the weld zones are small for the evenly loaded copper shell. The maximum values are about 0.04 (4%), see Figure 3-12. These values are only present close to the slit roots. In the rest of the weld zone the strains are below 0.01. For uneven load cases, the plastic strains in the upper weld zones remain small; the maximum values are only 0.01, see Figures 3-13 and 3-14. However, the plastic strains in the lower weld zones approach 0.10 and 0.13 for load case 1 and 2, respectively, but are well below 0.02 in the rest of the weld zones.

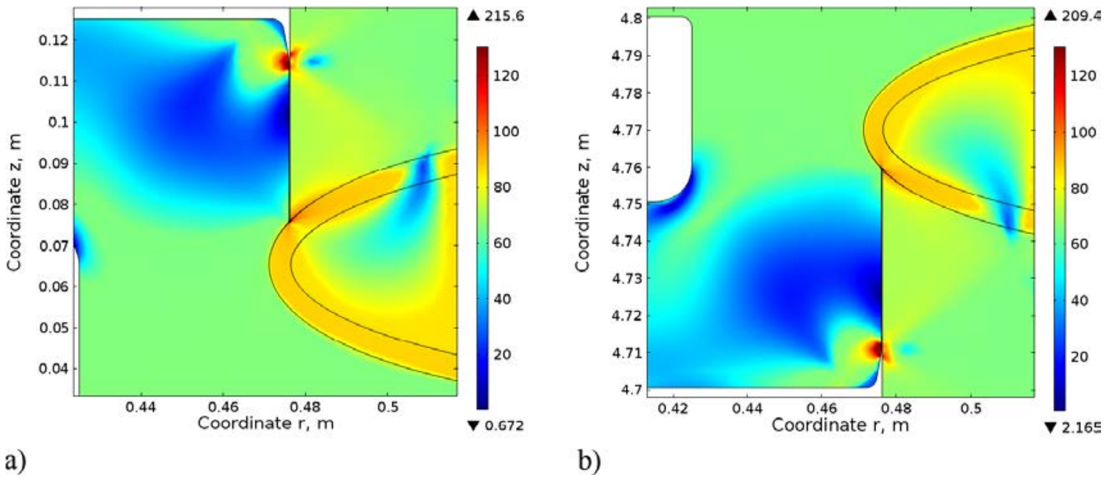

***Figure 3-9.** von Mises stress (MPa) in and around the weld zones for load case 0; a) base weld; b) lid weld.*

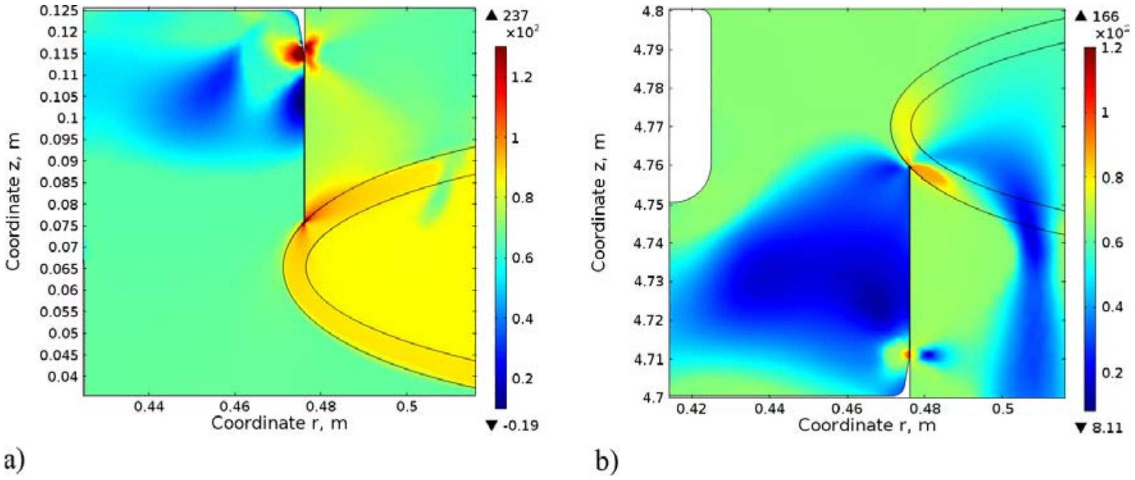

Figure 3-10. *von Mises stress (MPa) in and around the weld zones for load case 1; a) base weld; b) lid weld*

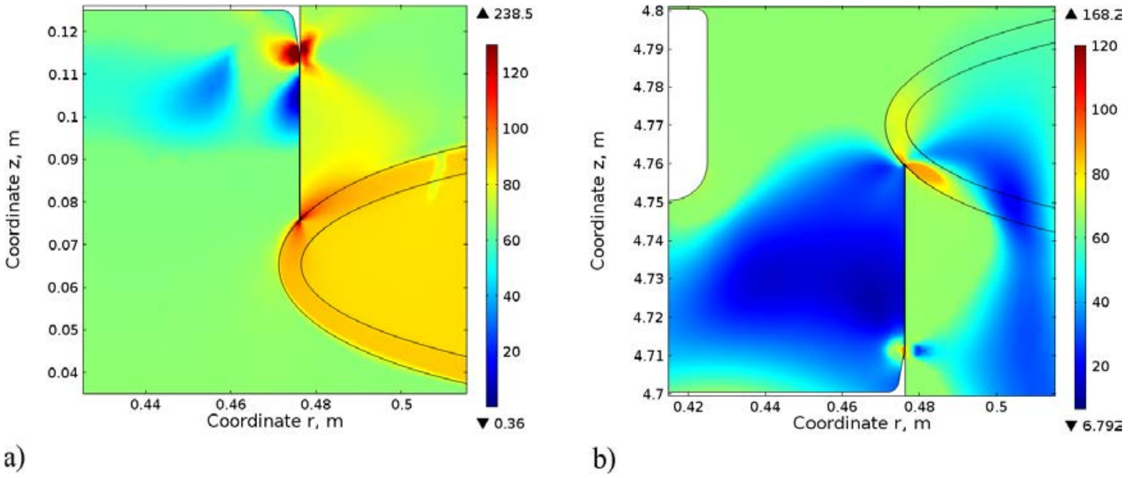

Figure 3-11. *von Mises stress (MPa) in and around the weld zones for load case 2; a) base weld; b) lid weld*

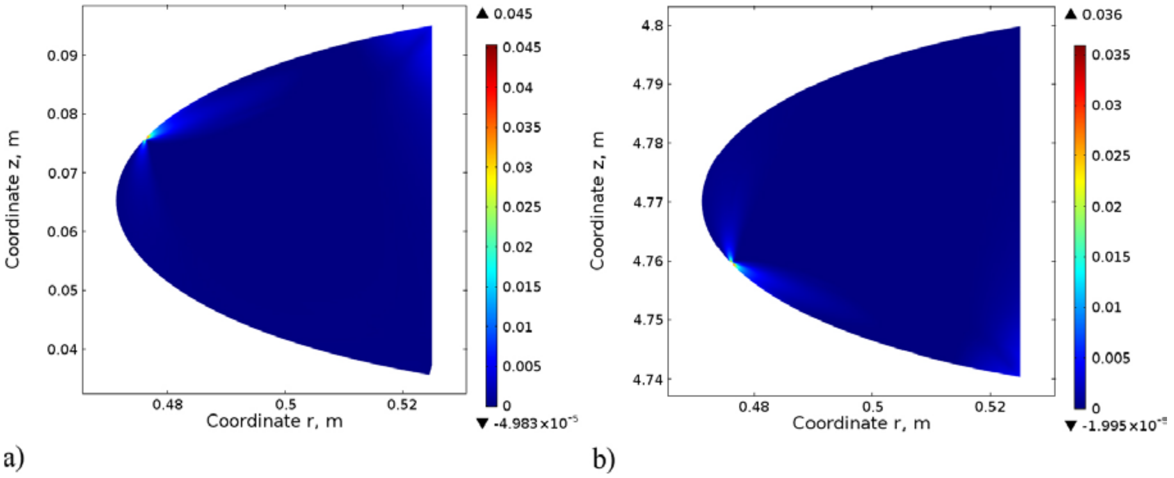

Figure 3-12. *Plastic strain distribution in the welds for load case 0; a) base weld; b) lid weld.*

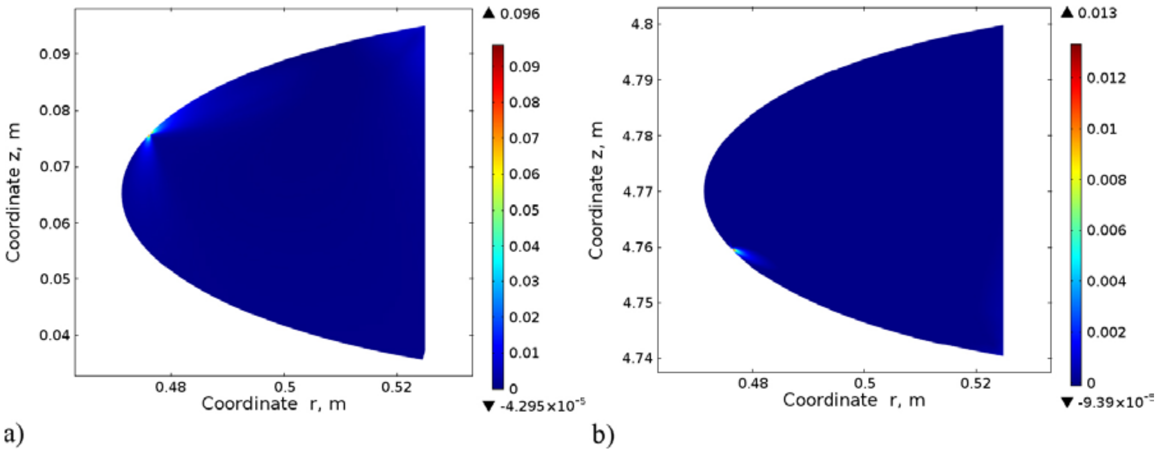

Figure 3-13. *Plastic strain distribution in the welds for load case 1; a) base weld; b) lid weld.*

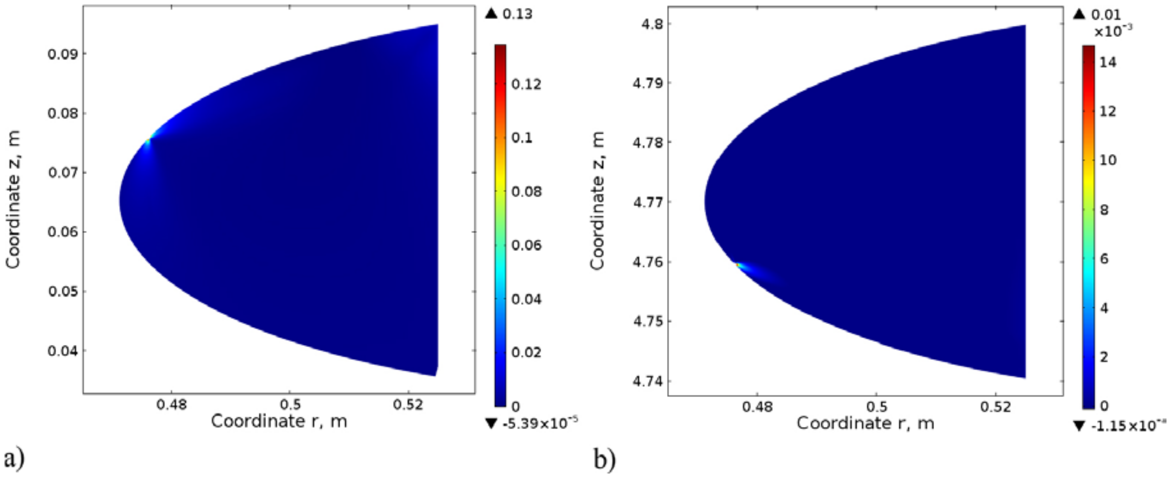

Figure 3-14. *Plastic strain distribution in the welds for load case 2; a) base weld; b) lid weld.*

It is evident that the von Mises stresses in each load case do not vary much across the weld zone and their magnitudes are not very high. The balanced properties of the parent metal, HAZ, and TMAZ imply that the stress concentration is not sufficient to give rise to local plastic deformation and to threaten the integrity of the copper shell.

3.4 Slits

Load case 0. Homogeneous loading

An overview of the von Mises stress distribution around the slits is presented in Figure 3-9. No contact occurs between the sides of the slits except at positions of about 10 mm from the entrance to the upper and lower slits. The corresponding contact stresses across the slits are shown in Figure 3-15.

Figure 3-15 shows that the maximum von Mises stresses that appear are 158 MPa in the lower slit and 172 MPa in the upper one. The maxima appear at the contact positions. These stresses are compressive. The contact stresses in Figure 3-15 are lower than the corresponding maximum legend stresses in Figure 3-9. Compared with the enlarged views of the slit roots in Figure 3-16, it is obvious that the largest stresses lie at the slit roots in touch with HAZ. The maximum stresses are 216 MPa.

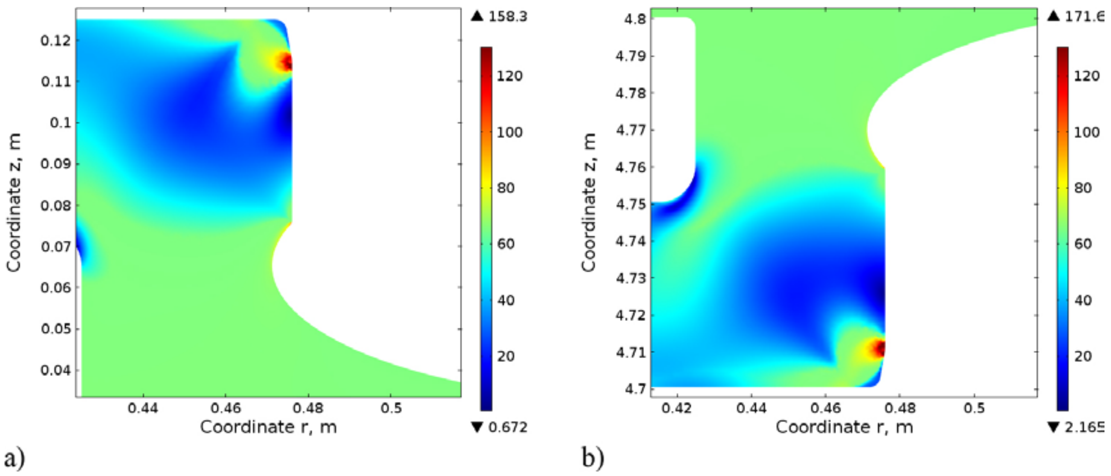

Figure 3-15. *Contact stress (von Mises, MPa) across the slits for load case 0; a) inner contact part in the lower slit; b) inner contact part in the upper slit.*

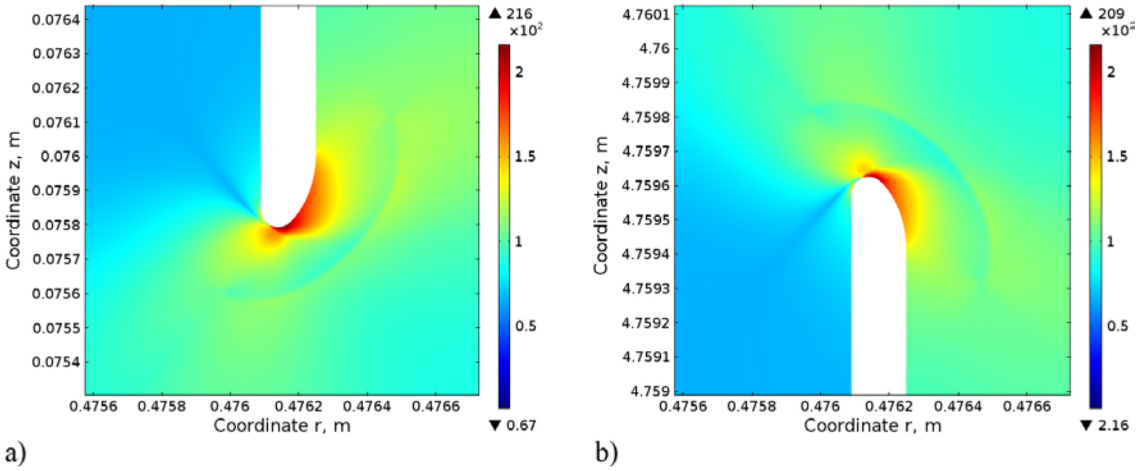

Figure 3-16. *von Mises stress distribution in MPa around the slit roots for load case 0; a) lower slit root; b) upper slit root.*

Figure 3-17a shows the plastic strains in the lower slit root. Right at the bottom of the slit root plastic strains as high as 0.52 (52%) are present. However, the stresses in the slit root are compressive and no creep damage will develop. The radial stress distribution can be seen in Figure 3-17b. This is the stress component that is perpendicular to the slit.

The situation is the same for the upper slit root, Figure 3-18. There are high local strains but the stresses at the slit root are compressive. Tensile stresses of up to 100 MPa appear at the sides of the slit, but stresses at that level are too low to generate creep damage. A stress of 100 MPa gives a creep strain of $3 \cdot 10^{-5}$ at 75°C after one million years, which is totally negligible. The model used has been verified experimentally at such low stresses (Sandström 2012).

The circumferential stress component is shown in Figure 3-19. The maximum legend tensile stresses of about 85 MPa in the upper and lower slit roots are not sufficiently high to initiate creep damage.

The axial stress components (not shown) are low in the slit roots and are of no significance.

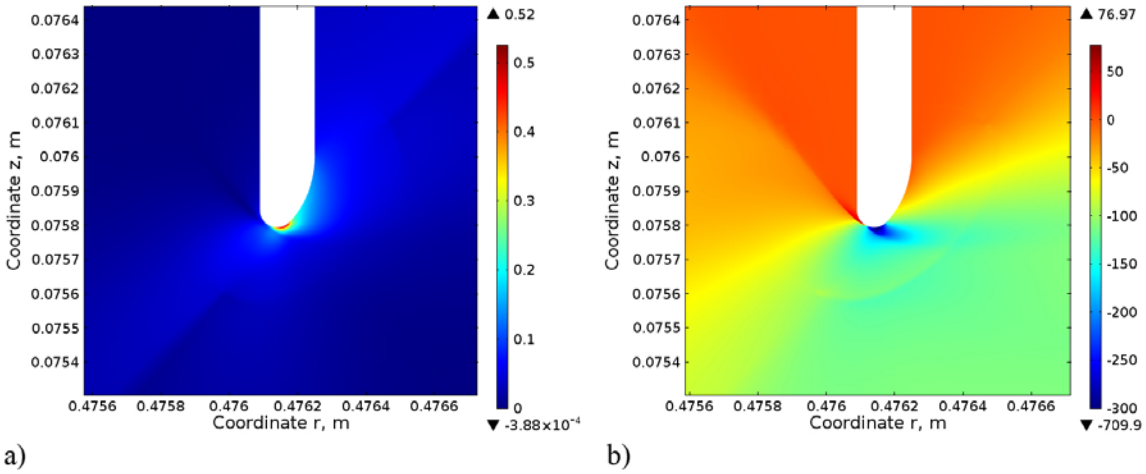

Figure 3-17. *Lower slit root for load case 0; a) plastic strain distribution; b) distribution of radial stress in MPa.*

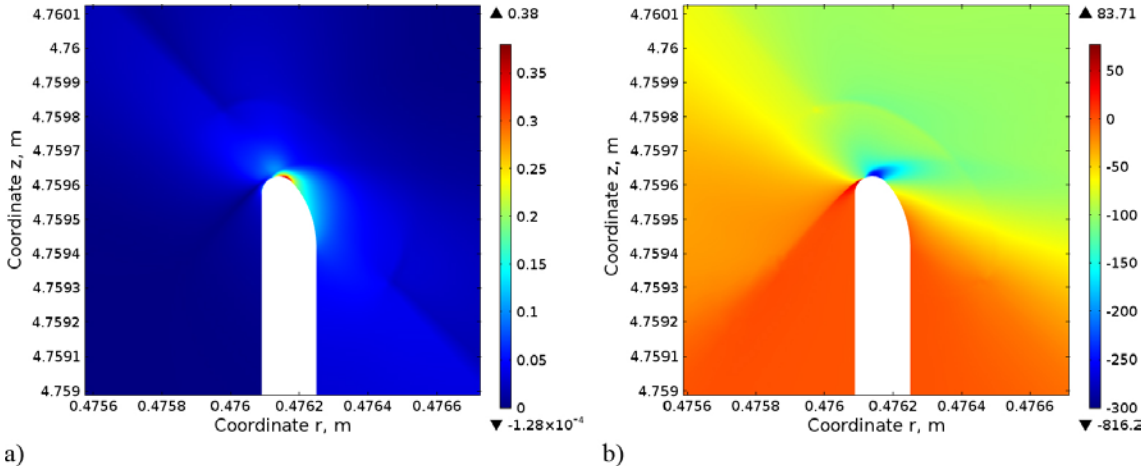

Figure 3-18. *Upper slit root for load case 0; a) plastic strain distribution; b) distribution of radial stress in MPa.*

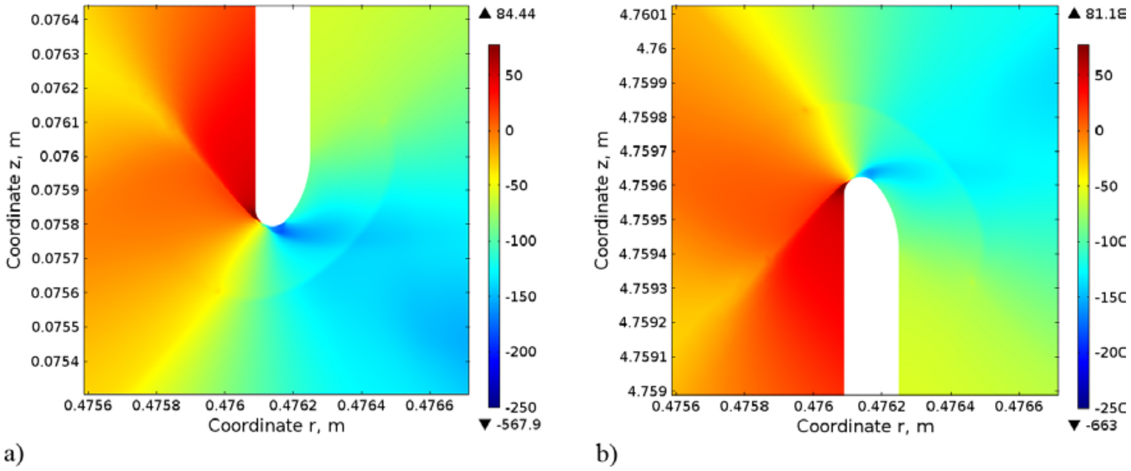

Figure 3-19. *Distribution of circumferential stress in MPa for load case 0; a) lower slit root; b) upper slit root.*

Load case 1. Shear stress along all of the shell

The von Mises stress distribution around the slits is presented in Figure 3-10. The corresponding contact stresses across the slits are shown in Figure 3-20.

This figure shows that the maximum von Mises stress is 161 MPa. The maximum appears at a contact position, where the radial stress is compressive. All of the contact stresses in Figure 3-20 are lower than the corresponding maximum legend stresses in Figure 3-10. The largest stresses lie at the bottom of the slit roots, Figure 3-21.

Figure 3-22a shows the plastic strains around the lower slit root. Plastic strains as high as 0.67 are found. Again the radial stresses are compressive at the slit root, Figure 3-22b, so no creep damage will be generated.

The strain and radial stress distributions in the upper slit root are shown in Figure 3-23. High strains but again compressive stresses are found, so the situation is the same as for the lower slit root. Tensile stresses of up to 80 MPa appear on the sides of the slits, but these are too low to generate creep damage.

The circumferential stress components are shown in Figure 3-24. The maximum legend tensile stresses is 77 MPa in the lower slit root and again that is not sufficient to initiate creep damage. In the same way as in load case 0, the axial stress components (not shown) is low at the slit roots.

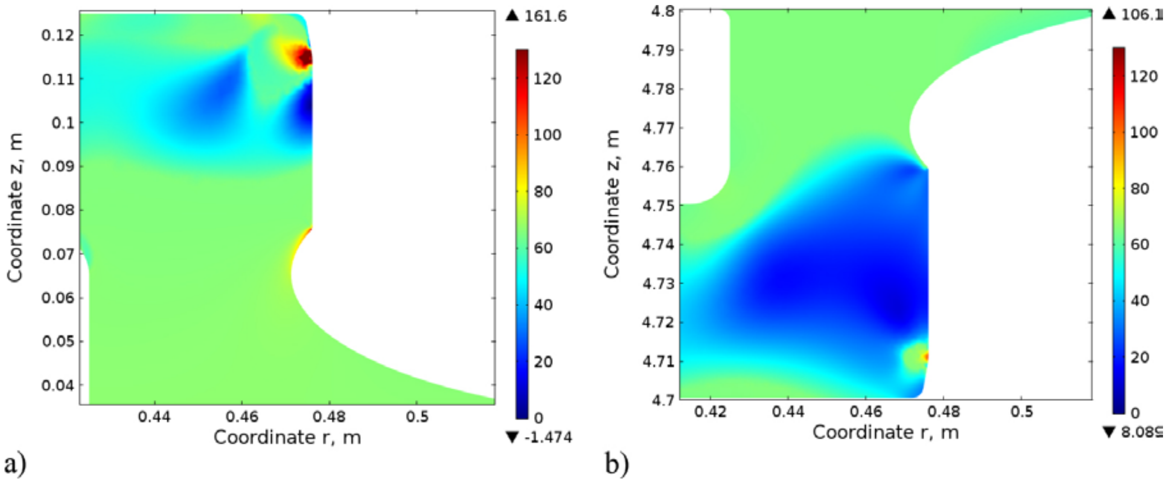

Figure 3-20. *Contact stress (von Mises, MPa) across the slits for load case 1; a) inner contact part in the lower slit; b) inner contact part in the upper slit.*

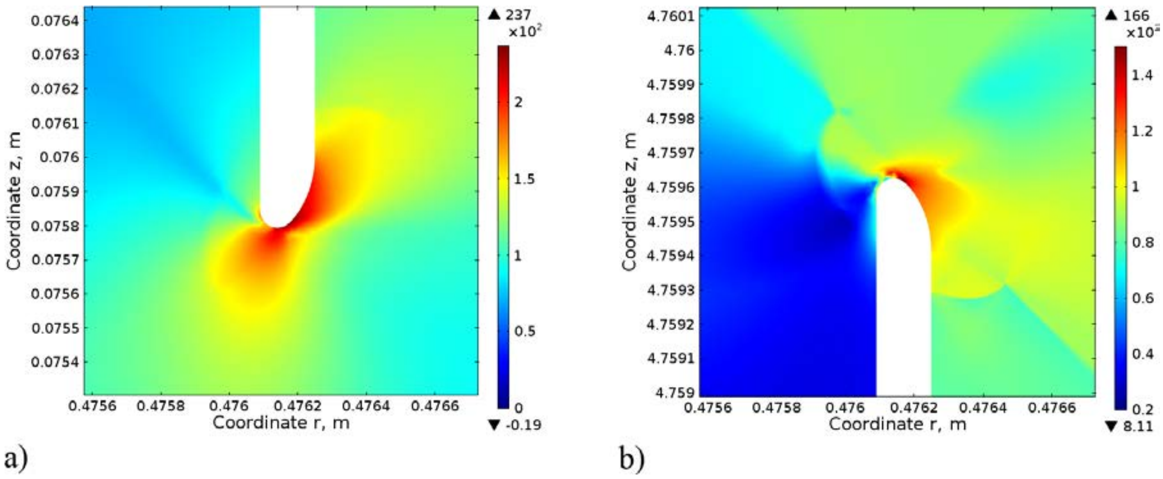

Figure 3-21. *von Mises stress distribution in MPa around the slit roots for load case 1; a) lower slit root; b) upper slit root.*

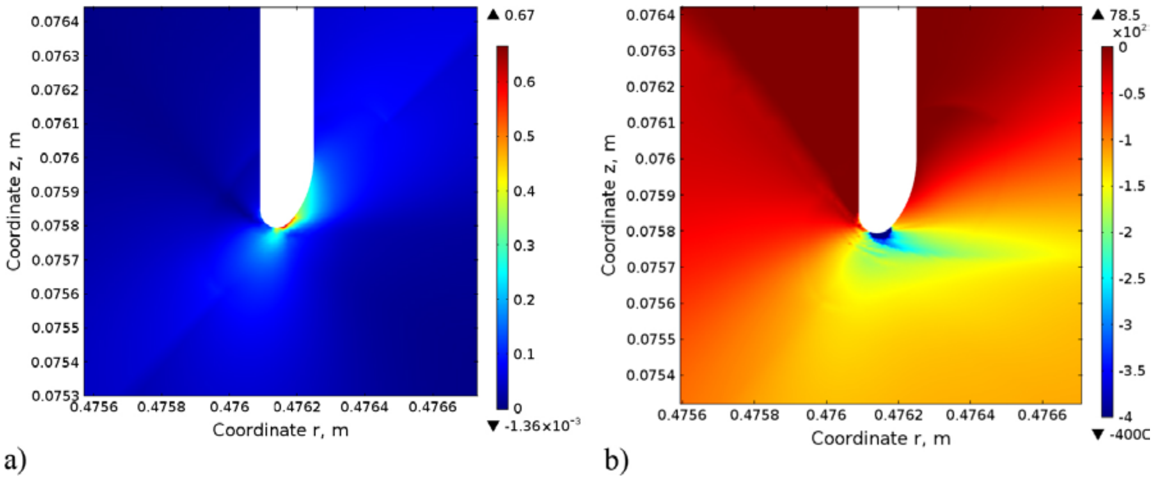

__Figure 3-22.__ Lower slit root for load case 1; a) plastic strain distribution; b) distribution of radial stress in MPa.

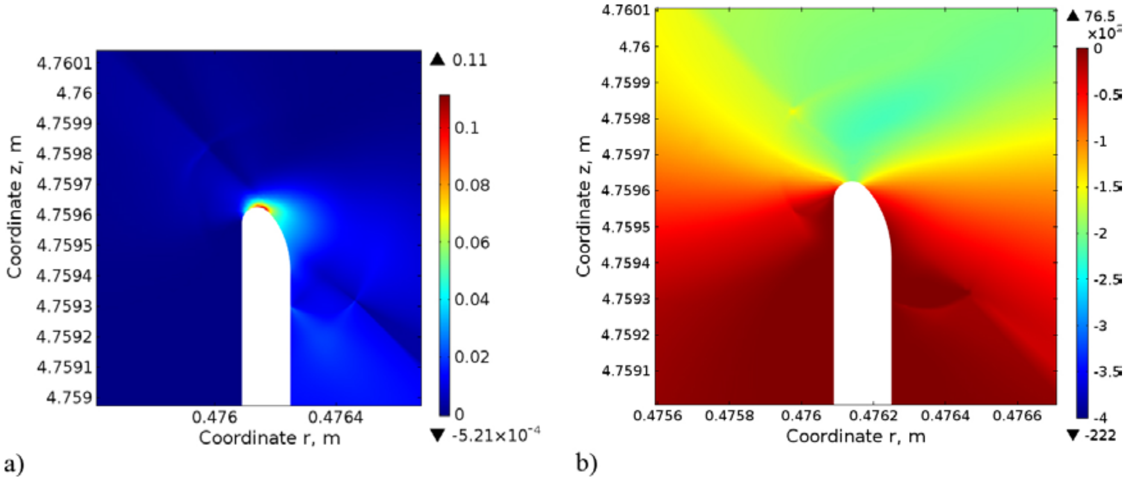

__Figure 3-23.__ Upper slit root for load case 1; a) plastic strain distribution; b) distribution of radial stress in MPa.

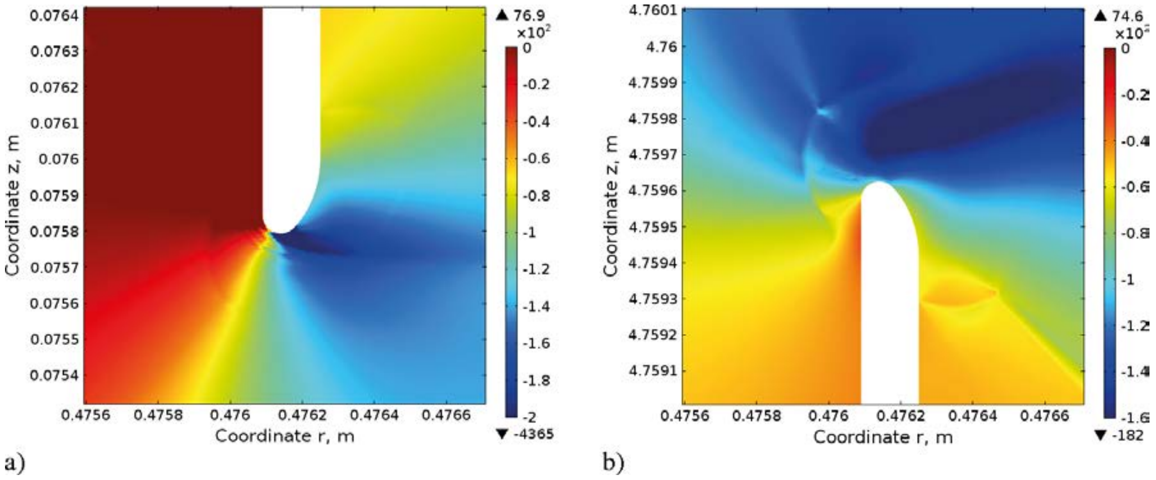

__Figure 3-24.__ Distribution of circumferential stress in MPa for load case 1; a) lower slit root; b) upper slit root.

Load case 2. Shear stresses along the bottom part of the shell

An overview of the von Mises stress around the slits is given in Figure 3-11. The contact stresses across the slits are shown in Figure 3-25. This shows that the maximum stresses are 186 MPa in the lower slit and 99 MPa in the upper one. These maxima appear at the contact positions and these stresses are compressive. The non-homogeneous external loading gives a large difference in stresses in the upper and lower parts of the copper shell.

If the contact stresses in Figure 3-25 are compared with stresses in the slit roots in Figure 3-26, it is obvious that the largest stresses are located at the slit roots in the same way as in load case 0 and 1. In the lower slit root the maximum stress is 238 MPa.

Figure 3-27a shows that the plastic strain can reach values as high as 0.74 in the lower slit root. Again the stresses are compressive in this region, Figure 3-27b.

The situation at the upper slit root is illustrated in Figure 3-28. Again the stresses are compressive at the slit roots.

The circumferential stress components are shown in Figure 3-29. The maximum legend tensile stress is 76 MPa in the lower slit root, which is not enough to initiate creep damage. The axial stress components (not shown) are low in the slit roots.

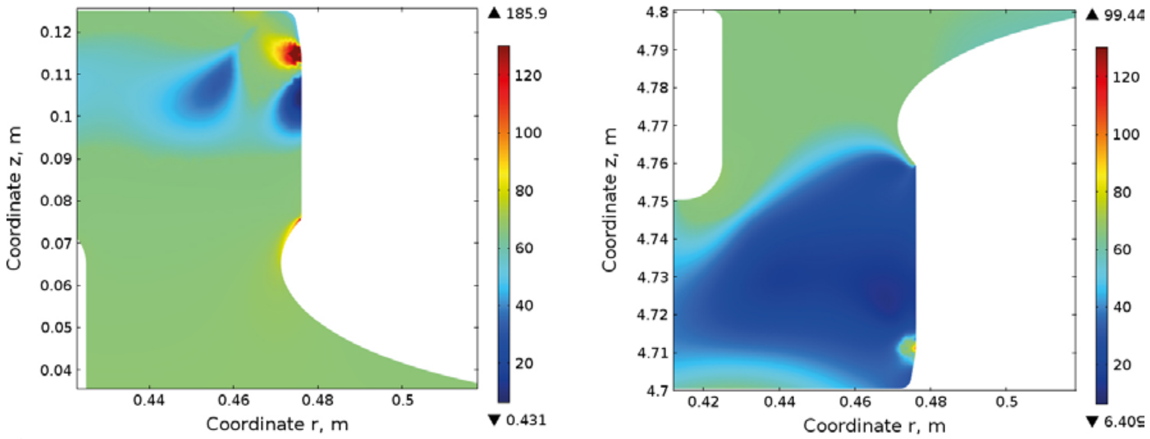

a) b)

Figure 3-25. *Contact stress (von Mises, MPa) across the slits for load case 2; a) inner contact part in the lower slit; b) inner contact part in the upper slit.*

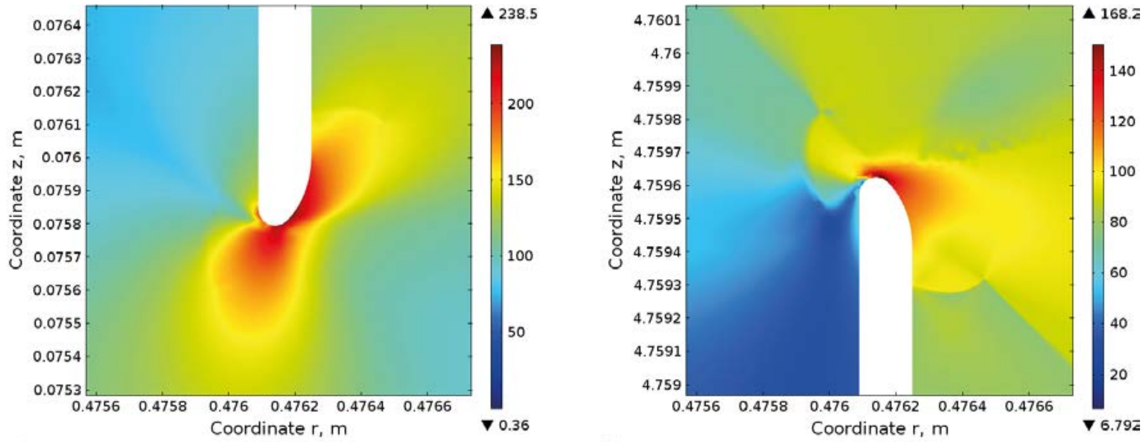

a) b)

Figure 3-26. *von Mises stress distribution in MPa around the slit roots for load case 2; a) lower slit root; b) upper slit root.*

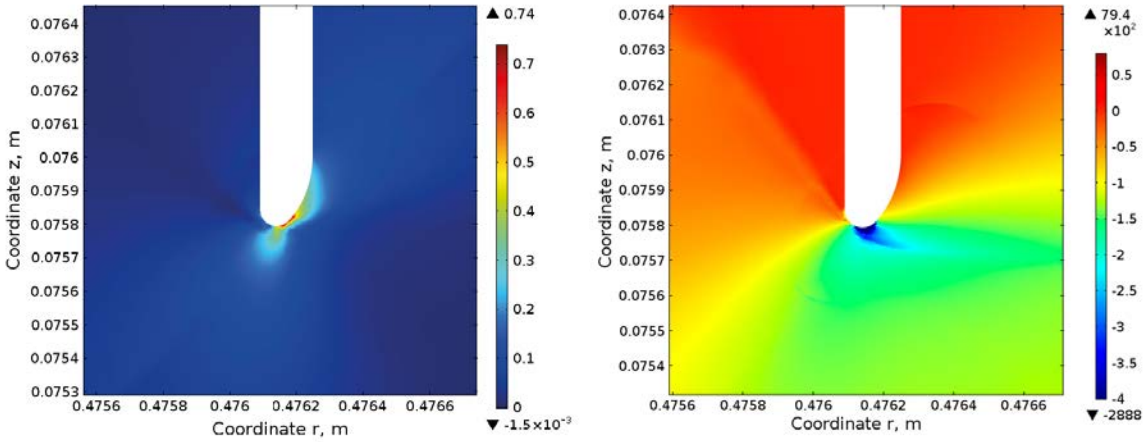

a) b)

Figure 3-27. *Lower slit root for load case 2; a) plastic strain distribution; b) distribution of radial stress in MPa.*

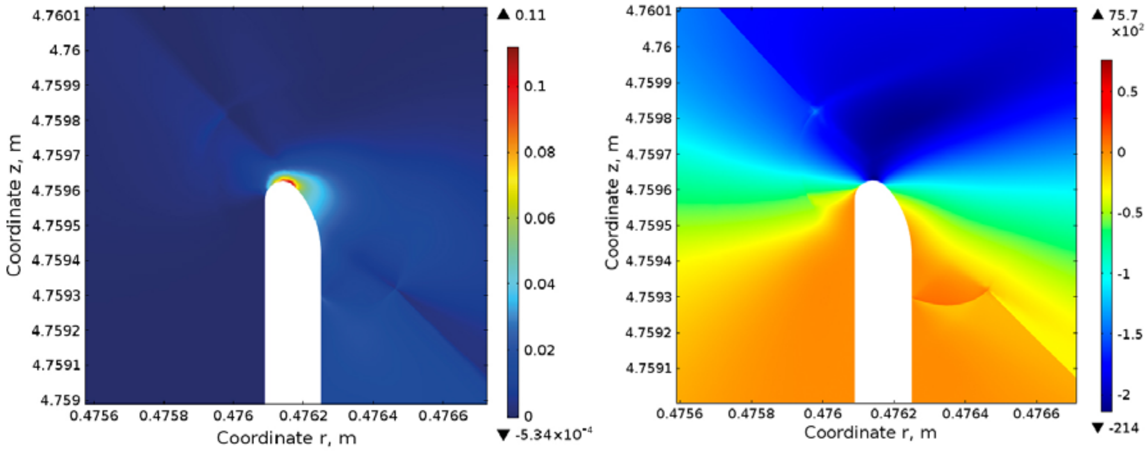

a) b)

Figure 3-28. *Upper slit root for load case 2; a) plastic strain distribution; b) distribution of radial stress in MPa.*

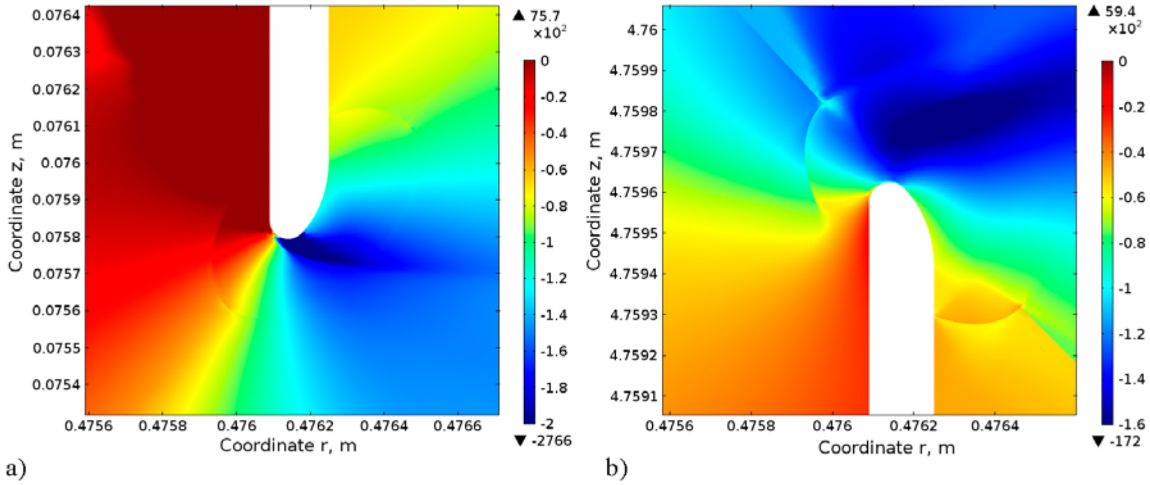

a) b)

Figure 3-29. *Distribution of circumferential stress in MPa for load case 2; a) lower slit root; b) upper slit root.*

Comparison between the load cases 0, 1 and 2

The general behaviour of the stress and strain distributions in the three load cases is quite similar. The local stresses and strains are largest in load case 2. This is an effect of the large shear stress gradient in the lower part of the copper shell for this load case. In all three load cases there are local regions in the bottom of the slits where the strains take high values. However, for both the lower and upper slit roots in all three load cases, the stresses are compressive at these positions and no creep damage will be generated.

4 Discussion

The present computations are carried out for one even and two uneven load distributions, which are referred to as load case 0, 1, and 2. The even load distribution is expected to represent the most common situation. However, uneven load distributions might appear, for example as the result of rock fall out. In load case 0, a uniform pressure of 15 MPa is acting on the copper shell surface. In both load cases 1 and 2, the pressure at the top of the copper shell is 7.4 MPa and the pressure at the base 19 MPa. However, different pressure gradients are utilised along the surface of the copper cylinder. The chosen loadings for load case 1 and 2 should correspond to the worst-case situations (SKBdoc 1206894). In the modelling, the parent and friction stir welded Cu-OFP undergo isotropic strain hardening with a strain rate of $1 \cdot 10^{-8}$ s^{-1} (Sandström et al. 2013b). The elasto-plasticity model describes the stress strain evolution in the friction stir welded copper shell corresponding to one year's incremental loading. It means that stress relaxation has been fully taken into account.

The computation indicates that already an external pressure of 0.36 MPa generates an observably inward displacement in the lid/base and cylinder wall. The inner surface of the lid/base has touched the cast iron insert under a pressure of about 1.2 MPa at the axial symmetry axis. Similar actions take place in the copper cylinder when the external pressure exceeds 7.5 MPa for load case 0, 7.8 MPa for load case 1 and 8.1 MPa for load case 2, see Figures 3-5 to 3-7. There is no contact on the copper cylinder at the axial z-coordinate of 1.96 m and above for load case 2.

The initiation of plastic yielding in the lid and base begins at pressures of 3.4 and 3.8 MPa respectively at a distance of about 0.2 m from the copper shell axis. For the copper cylinder, the inward deflection of up to about 0.2 mm remains essentially elastic in nature. A detectable plastic yielding occurs in the copper cylinder only when the pressure approaches 6.7 MPa. These critical pressures are the structural characteristics of the copper shell, irrespectively of whether the load is even or uneven. It suggests that the lid/base will come into a state of plastic yielding much earlier than the cylinder during incremental loading.

The plastic yielding in the copper cylinder and the lid/base inevitably gives rise to contour distortion in the slits. Compared to the von Mises stress of 216 MPa and the average plastic strain of 0.23 (true strain) in the 15 MPa evenly loaded copper shell, the unevenly loaded cases enhance the bottom pressure to 19 MPa and reduce the top pressure to 7.4 MPa. Therefore, the most severely strained and stressed regions in the whole copper shell reside at the slit roots, particularly at the lower slit roots of the unevenly loaded copper shells, in touch with the HAZ. The difference in plastic strains in the lower slit roots may reasonably be associated with the swelling pressure gradients, being 2.39 MPa/m in load case 1 and 5.92 MPa/m in load case 2. A larger plastic strain originates from a strong stress concentration and subsequent stress relaxation. With a unique geometry constraint and a similar remaining stress (maximum von Mises stress) in the slit roots, it can be deduced that the stronger stress gradient acting around a lower slit will produce a more severely stress concentrated region and thus a larger remaining plastic strain than a weaker one.

As suggested by the constitutive equations (Sandström et al. 2013b), the difference in properties between parent metal, HAZ, and the centre part of the weld zone, the thermally affected zone, TMAZ, is comparatively small. von Mises stresses in the range of 40–90 MPa are smoothly distributed in the upper and the lower friction stir welded zones. The stress variation between the welds and the parent metal can be attributed to the slightly higher strength of friction stir welds than that of parent Cu-OFP. Even though differences in yield strength and work hardening between the parent metal and the welds induce local stress variations, the stress transition between the parent metal and the welds is smooth and thus should be harmless to the copper shell integrity. The computed plastic strains in most of the weld zones are small, the maximum value is about 0.05. The exceptions are in the lower weld zones of unevenly loaded copper shells where plastic strains as high as 0.10 and 0.13, respectively, emerge, see Figures 3-13 and 3-14. Plastic strains of such magnitudes do not develop creep cracks (Wu et al. 2013).

For the first time a detailed stress analysis of the slits between the copper tube on one hand and the lid or base on the other hand has been performed. At the bottom of the slits narrow radii are present that give rise to stress concentrations. High von Mises stresses of up to 236 MPa have been found in the slit roots. These high stresses are associated to high local strains as well. The highest values are observed in the lower slit in load case 2. In both the upper and lower slit roots in all the three considered load cases, the stresses are compressive to the slits. This implies that no creep damage will be initiated. On the sides of slits there are tensile stress components in certain areas, but there size is not larger than 100 MPa and that is not sufficient to cause any creep damage.

5 Conclusions

With constitutive equations developed from slow strain rate tensile data on weld zones, elasto-plastic finite element analyses with contact modelling have been carried out to study the plastic deformation of copper shells under both even (load case 0) and uneven pressures (load case 1 and 2). A gradual loading has been assumed to simulate the expected conditions in the repository. The applied external pressure has been increased linearly with log time.

1. The deformed cylindrical copper shell in load case 0 and 1 takes an hourglass shape with lid/base behaving as inward clamped disks, which corresponds to the inward displacements of 1 mm in lid/base and 1.5 mm in copper cylinder. The deformation of copper shell in load case 2 with a larger shear stress gradient is characterised by the inward displacements of 1 mm in lid/base and the inward deflection of 1.5 mm in part of the copper cylinder. The deflection gives rise to a plastic strain up to 0.82% near the edge of the deflected inner base and cylinder wall, and to 0.54% in the middle of the inner base.
2. von Mises stresses up to 90 MPa are distributed in the lower and upper friction stir welded zones with smooth stress transition. The plastic strains are small in the weld zones (except at the slit roots). As a result, the welds will have insignificant effect on the copper shell integrity.
3. The most severely deformed sections in the whole copper shell lie in the slit roots, particularly in the lower slit roots of unevenly loaded copper shells. von Mises stresses up to 238 MPa emerge there. However, the stresses in the slit roots are compressive and no creep damage will be initiated. The larger stress gradient in load case 2 produces higher stress concentrations and larger plastic strains in the lower slit root than in load case 1.

Acknowledgements

The authors wish to thank the Swedish Nuclear Fuel and Waste Management Company (SKB) for its grant to this study. Valuable comments from Christina Lilja and Mikael Jonsson, SKB are gratefully acknowledged.

References

SKB's (Svensk Kärnbränslehantering AB) publications can be found at www.skb.se/publications. References to SKB's unpublished documents are listed separately at the end of the reference list. Unpublished documents will be submitted upon request to document@skb.se.

Andersson H C M, Seitisleam F, Sandström R, 2007. Creep testing and creep loading experiments on friction stir welds in copper at 75°C. SKB TR-07-08, Svensk Kärnbränslehantering AB.

Börgesson L, Johannesson L-E, Sandén T, Hernelind J, 1995. Modelling of the physical behaviour of water saturated clay barriers. Laboratory tests, material models and finite element application. SKB TR 95-20, Svensk Kärnbränslehantering AB.

Börgesson L, Dueck A, Johannesson L-E, 2010. Material model for shear of the buffer – evaluation of laboratory test results. SKB TR-10-31, Svensk Kärnbränslehantering AB.

Jin L-Z, Sandström R, 2008. Creep of copper canisters in power-law breakdown. Computational Materials Science 43, 403–416.

Jin L-Z, Sandström R, 2009. Non-stationary creep simulation with a modified Armstrong–Frederick relation applied to copper canisters. Computational Materials Science 46, 339–346.

Raiko H, Sandström R, Rydén H, Johansson M, 2010. Design analysis report for the canister. SKB TR-10-28, Svensk Kärnbränslehantering AB.

Sandström R, 2012. Basic model for primary and secondary creep in copper. Acta Materialia 60, 314–322.

Sandström R, Andersson H C M, 2008. Creep in phosphorus alloyed copper during power-law breakdown. Journal of Nuclear Materials 372, 76–88.

Sandström R, Hallgren J, 2012. The role of creep in stress strain curves for copper. Journal of Nuclear Materials 422, 51–57.

Sandström R, Östling H, Jin L-Z, 2013a. Modelling of creep in friction stir welded copper. Materials Research Innovations 17, 350–354.

Sandström R, Waqas Ahmad S, Pasupuleti K T, Mahdavi Shahri M, 2013b. Slow strain rate tensile testing of friction stir welded Cu-OFP. Constitutive equations for creep. SKB R-13-33, Svensk Kärnbränslehantering AB.

SKB, 2010. Design, production and initial state of the canister. SKB TR-10-14, Svensk Kärnbränslehantering AB.

Wu R, Sandström R, Jin L-Z, 2013. Creep crack growth in phosphorus alloyed oxygen free copper. Materials Science and Engineering A 583, 151–160.

Unpublished documents

SKBdoc id, version	Title	Issuer, year
1206894 ver 1.0	Uneven swelling pressure on the canister simplified load cases derived from uneven wetting, rock contours and buffer density distribution	SKB, 2009